Exchange-spring-driven spin flop in an $ErFe_2/YFe_2$ multilayer studied by x-ray magnetic circular dichroism

G. B. G. Stenning,[1,*] A. R. Buckingham,[1] G. J. Bowden,[1] R. C. C. Ward,[2] G. van der Laan,[3] L. R. Shelford,[3] F. Maccherozzi,[3] S. S. Dhesi,[3] and P. A. J. de Groot[1]

[1]*School of Physics and Astronomy, University of Southampton SO17 1BJ, United Kingdom*

[2]*Clarendon Laboratory, Oxford University OX1 3PU, United Kingdom*

[3]*Diamond Light Source, Chilton, Didcot OX11 0DE, United Kingdom*

(Received 26 November 2010; revised manuscript received 8 April 2011; published 15 September 2011)

X-ray magnetic circular dichroism at the Er $M_{4,5}$ edge is used to study the switching behavior of the hard $ErFe_2$ layers in an epitaxial [$ErFe_2$(70 Å)/YFe_2(150 Å)] × 25 exchange-spring superlattice. Magnetic hysteresis loops for the Er magnetization, at temperatures $T < 200$ K, reveal a single irreversible switch between a vertical exchange spring and its reversed state. Experiments at $T > 200$ K reveal a crossover to a regime with two irreversible switching processes. Computational modeling for this system gives good agreement with the experiment, revealing that the observed high-temperature switching behavior is due to an exchange-spring-driven spin-flop-like transition. In contrast to the conventional spin-flop transition in an antiferromagnet, the increase in anisotropy energy of the hard magnetic $ErFe_2$ layers and Fe-Fe exchange energy is overcome by a decrease in overall Zeeman energy. Computational studies also reveal two types of transitions between vertical exchange-spring and spin-flop states with first-order and second-order character.

DOI: 10.1103/PhysRevB.84.104428 PACS number(s): 75.25.−j, 75.60.Jk, 75.30.Gw, 75.75.−c

I. INTRODUCTION

Exchange-spring magnetic multilayers, consisting of alternating hard and soft magnetic layers, have attracted a great deal of attention for their potential applications in data storage media,[1–3] permanent magnets,[4,5] and MEMS.[6–8] Such multilayers have been proposed as superior data storage media because they offer additional flexibility in optimizing magnetic properties. For instance, they provide a degree of decoupling between the coercivity, which determines the required write field, and the energy barrier required to avoid thermally activated data loss.[1] In short, such systems may be used to overcome the super-paramagnetic limit. For such applications, it is important to develop a detailed understanding of the magnetization switching in exchange-spring structures.

In recent years, it has been shown that multilayer films of Laves phase $REFe_2$ (RE = rare earth) grown by molecular beam epitaxy (MBE) are excellent model systems for the study of exchange-spring phenomena.[9] In two earlier papers, the magnetic properties of MBE-grown $ErFe_2/YFe_2$ superlattices were reported and discussed.[10,11] In particular, magnetic measurements, complimented by micromagnetic modeling, were used to show that at low temperatures, $T \leqslant 200$ K, the easy axis lies between the [110] crystal growth axis and an out-of-plane ⟨111⟩ axis. The direction of easy magnetization is determined primarily by the cubic crystal field interaction at the Er^{3+} site, which favors ⟨111⟩ axes. However in MBE-grown (110) $ErFe_2$ films, there is an additional strain term to the magnetic anisotropy, which favors the crystal growth axis.[12] Consequently, at low temperatures, the easy axis is out of plane, between either the [111]−[110] or [11$\bar{1}$]−[110] axes, with no y-component ([$\bar{1}$10]). The situation is illustrated schematically in Fig. 1(a). Note that in the presence of a field applied along the [110] growth axis, a magnetic exchange spring is set up in the soft YFe_2 layer. We shall refer to such a spin state as a *vertical exchange spring*, given that the Er spins are constrained to lie close to the film normal.

From bulk magnetometry and anomalous Hall effect measurements at low temperatures,[10,11] it is known that there is just one irreversible switch of the hard layers from, say, a near [11$\bar{1}$] axis to a near [$\bar{1}\bar{1}\bar{1}$] out-of-plane axis on the reverse side of the film. This results in a relatively simple M-B_a magnetic loop. However, at higher temperatures in excess of 200 K, there is an additional irreversible switch at fields ∼6 T, involving some kind of reorientation. Computational studies show that this can be explained if the direction of the Er magnetization flips from being near a ⟨111⟩ *out-of-plane* direction to a near *in-plane* ⟨111⟩ direction.[10,11] The latter is illustrated in Fig. 1(b). We shall refer to this spin configuration as the *spin-flop state*. Note that the vertical exchange-spring and spin-flop states both attempt to minimize their Er anisotropy energies by exploiting near ⟨111⟩ easy cubic crystal field directions.

From computational studies, therefore, it is clear that the exchange-spring-driven spin-flop transition at high temperatures is characterized by a dramatic switch in the direction of the Er magnetic moments. This is in marked contrast to bulk magnetometry on $ErFe_2/YFe_2$ superlattices, which reveals only a weak magnetic signature, due to partial cancellation of Er and Fe net magnetic moments (see Fig. 3(b) of Ref. 10 and Fig. 1(c) of Ref. 11). Thus it is of interest to perform element-specific Er x-ray magnetic circular dichroism (XMCD). Indeed, similar XMCD measurements on $DyFe_2/YFe_2$ superlattices[13,14] have demonstrated the power of element-specific magnetometry. In the case of $DyFe_2/YFe_2$, which has near in-plane magnetic anisotropy, Dy-XMCD has revealed intricate magnetization reversal processes, in good agreement with computational studies.[15] Here we show that (i) Er-XMCD also offers profound information about the hysteretic processes in $ErFe_2/YFe_2$ multilayers, and (ii) the high-temperature

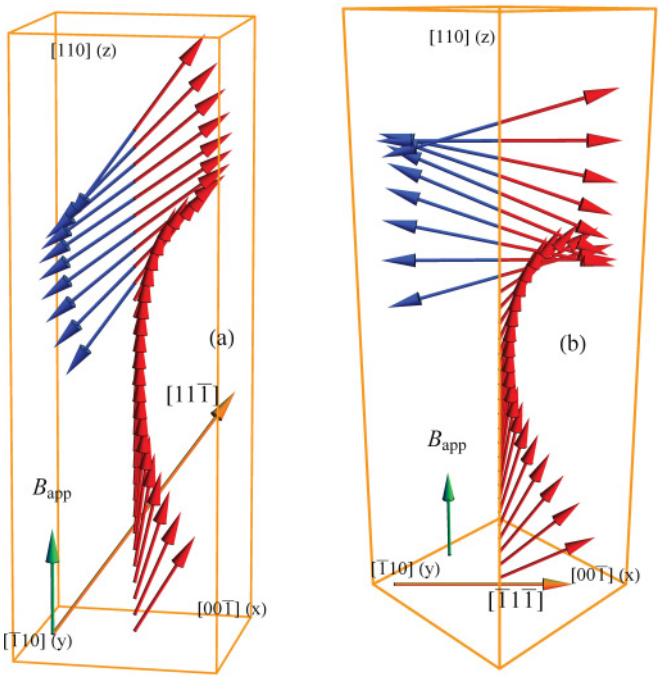

FIG. 1. (Color online) Calculated exchange-spring states in a field of 4 T at a temperature of 220 K. Blue/red arrows represent Fe/Er magnetic moments, respectively. (a) Vertical exchange-spring state, all spins confined to the ($\bar{1}$10) plane (no y component). (b) Spin-flop exchange-spring state, all spins confined to a near ($\bar{1}$12) plane (nonzero x and y components). For clarity, only every other magnetic monolayer is shown. Note rotation of 3D box by 45° about the z-axis ([110]), in going from Figs. 1(a) to 1(b).

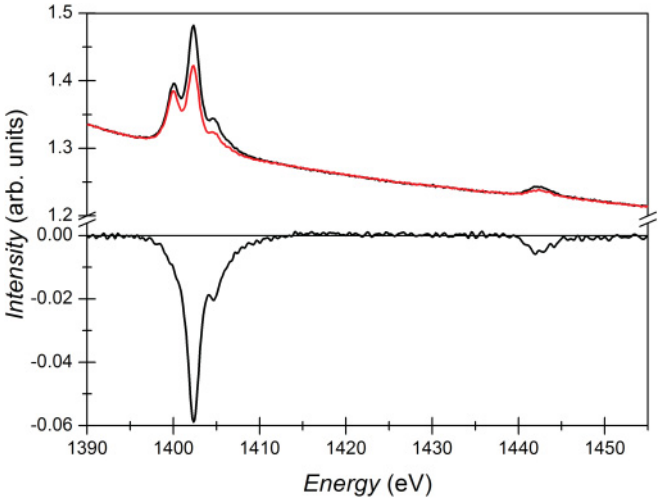

FIG. 2. (Color online) Er $M_{4,5}$ X-ray absorption spectra (XAS) in the energy range 1390–1450 eV, for both right-handed (upper/black) and left-handed (lower/red) circularly polarised light. This data was obtained using total electron yield. The difference curve (the XMCD) can be seen in the lower half of the diagram.

magnetic switching process is intimately associated with *saddle points* in the anisotropy surface of the Er^{3+} ion.

II. EXPERIMENTAL PROCEDURE

The $ErFe_2/YFe_2$ superlattice samples were grown by MBE following the procedure detailed in Refs. 16 and 17. A 100-Å Nb buffer layer and 20-Å Fe seed layer were deposited onto an epi-prepared (11$\bar{2}$0) sapphire substrate of size 10 mm × 12 mm. The Laves phase film consisted of a superlattice of [$ErFe_2$(70 Å)/YFe_2(150 Å)] × 25 grown with a (110) film plane and the major axes parallel to those of Nb. This was achieved by co-deposition of elemental fluxes at a substrate temperature of 600 °C. This substrate temperature has been shown to be optimum by x-ray reflectivity studies.[17] The mosaic spread is less than 0.9° (Ref. 16), the interface roughness is 7(1) Å with no significant interlayer diffusion.[17] To prevent the oxidation of the multilayer, the sample was capped with a 100-Å layer of Y.

XMCD measurements were performed on the soft x-ray undulator beamline I06 at Diamond Light Source (Chilton, Didcot, UK). The beamline is equipped with a superconducting magnet in a high vacuum of 10^{-10} mbar. Field sweeps were conducted between ±6 T in the temperature range 50–250 K to observe the exchange-spring-driven magnetization transitions. The magnetic field was applied parallel to the x-ray beam. The Er-XMCD signal was obtained as the difference in absorption between left- and right-circularly polarized x rays. An example, obtained using the Er $M_{4,5}$ ($3d \rightarrow 4f$ at 1405, 1440 eV), can be seen in Fig. 2 (see also Ref. 18). The difference signal (magnetic dichroism) can be used to measure the magnetic component of the Er magnetization in the direction of the incident x-ray beam. In initial experiments, the film normal was aligned 10° away from the x-ray beam direction. This geometry allowed for both x-ray fluorescence and electron drain current detection, but yielded practically identical Er-XMCD data.

XMCD results were also obtained using the Fe $L_{2,3}$ ($2p \rightarrow 3d$ at 710, 722 eV) transitions[19] and the Y $M_{2,3}$ (300, 310 eV) absorption edge. The latter did not show any magnetic circular dichroism; which we attribute to the presence of the non-magnetic Y capping layer. However, in the case of the Fe signal, pronounced Fe-XMCD was observed, but with low switching fields. This is consistent with signal originating from the last *magnetically free* YFe_2 layer.

For present purposes, therefore, only Er-XMCD experiments were performed using Er M_5 ($3d \rightarrow 4f$ at 1405 eV). Moreover, to simplify analysis of the experimental data, the sample was reoriented with the film normal parallel to the magnetic field and x-ray beam, and only total electron yield (TEY) was used to collect the experimental data.

III. ER-XMCD RESULTS

The Er-XMCD magnetization loops at various temperatures can be seen in Figs. 3 and 4. At temperatures of less than 200 K (Fig. 3), the Er-XMCD data are characterized by a single switching event, resulting in a simple magnetic loop. These data are consistent with bulk magnetometry. The gradual change of M_{Er} near $B_a = 0$ can be explained by the small rotation of magnetization from the easy axis to the film normal.

However, as the temperature is raised, a crossover between the single-switch behavior of Fig. 4(a) to the double-switch

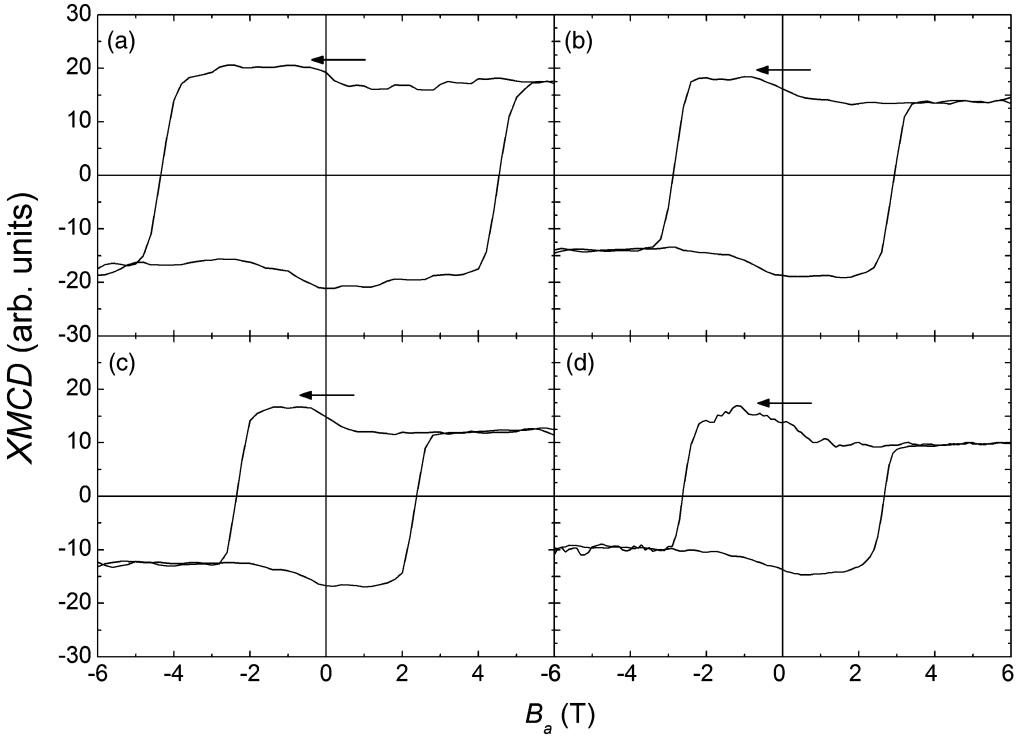

FIG. 3. M_{Er} hysteresis loops obtained by XMCD using total electron yield at (a) 50 K, (b) 100 K, (c) 150 K, and (d) 200 K.

behavior of Fig. 4(c) is observed. Upon further increase of temperature, the switching processes become better defined, and the M_{Er} hysteresis loops reveal two very distinct irreversible switching events at 250 K [Fig. 1(d)]. The low-field transition takes place at 0.4 T, whereas the high-field transition occurs at 3 T. The value of the latter is found to increase with increasing temperature.

As we shall see, an explanation of this complex switching behaviour can be provided by the discrete micromagnetic model described below.

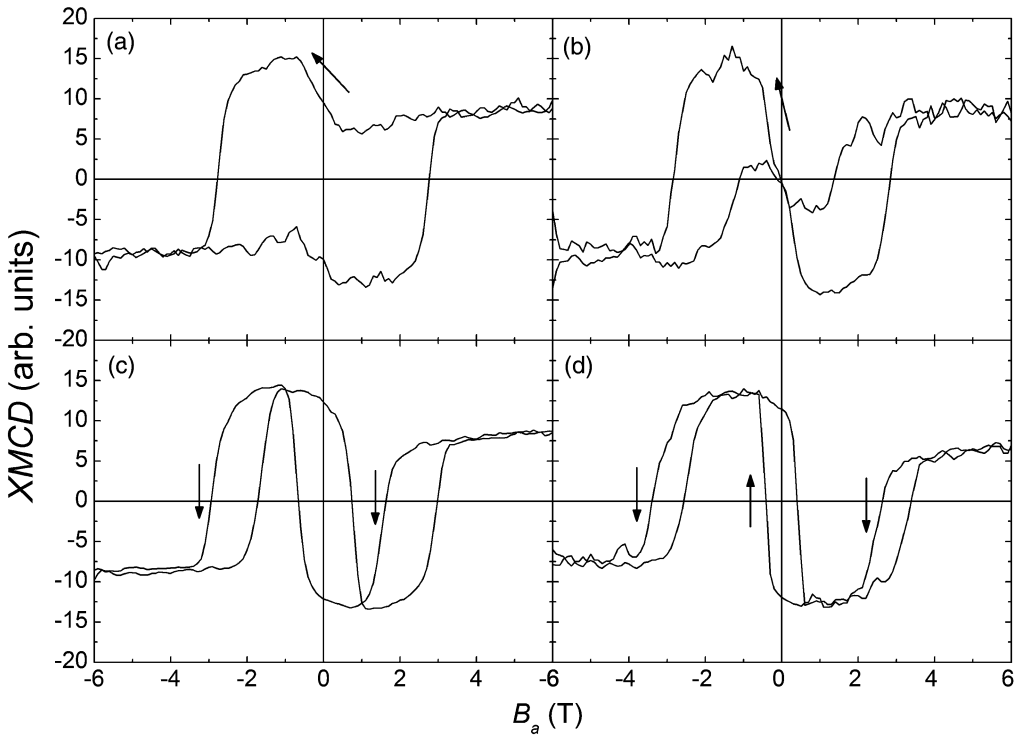

FIG. 4. M_{Er} hysteresis loops obtained by XMCD using total electron yield at (a) 215 K, (b) 220 K, (c) 225 K, and (d) 250 K.

IV. MICROMAGNETIC MODELING: THE DISCRETE MODEL

From a magnetic point of view, the magnetic exchange interactions can be categorized as follows. The strongest coupling is that of the ferromagnetic (FM) Fe-Fe exchange (∼600 K), which determines the high Curie temperatures of all the $REFe_2$ compounds. Next, is the anti-ferromagnetic (AFM) Er-Fe exchange (∼100 K). Finally, the Er-Er exchange is small and is neglected in the simulations described below. At $T =$ 0 K, the effective magnetic moments on the Er and Fe sites can be set at $9\mu_B$ and $1.5\mu_B$, respectively.[20] This approach is an oversimplification because band structure calculations have revealed that, in addition to the 3*d* moments on the iron, there are induced 5*d* moments at the RE sites.[21] However, because the 5*d* moments are driven primarily by the Fe 3*d* sublattice, it is a reasonable approximation to use a discrete two-component ferrimagnetic model, provided we ascribe $\mu_{\rm Er} = 9\mu_B$ and $\mu_{\rm Fe}(= \mu_{3d} + \mu_{5d}) = 1.5\mu_B$.[19]

Following Ref. 22, in discrete atomic form, the energy of an exchange spring takes the form

$$E_{\rm tot} = \sum_i^N \sum_j^N \sum_k^N \varepsilon_{i,j,k}, \tag{1}$$

where the energy $\varepsilon_{i,j,k}$ at site (i,j,k) is given by:

$$\begin{aligned}\varepsilon_{i,j,k} = &-\tfrac{1}{6}(2\mu_{\rm FE})B_{\rm EX}[\cos(\Omega_{i,j,k+1} - \Omega_{i,j,k}) \\ &+ \cos(\Omega_{i,j,k} - \Omega_{i,j,k-1}) + \cos(\Omega_{i,j+1,k} - \Omega_{i,j,k}) \\ &+ \cos(\Omega_{i,j,k} - \Omega_{i,j-1,k}) + \cos(\Omega_{i+1,j,k} - \Omega_{i,j,k}) \\ &+ \cos(\Omega_{i,j,k} - \Omega_{i-1,j,k})] + K_{i.j.k}(\Omega_{i,j,k}) \\ &- 2\mu_{\rm Fe}B_A\cos(\Omega_{i,j,k} - \Omega_H) + \mu_{\rm Er}B_A\cos(\Omega_{i,j,k} - \Omega_H)\end{aligned} \tag{2}$$

Here, we have (i) used a cubic lattice, with nearest neighbor interactions, (ii) set the energy at a given site equal to that of a formula unit (one Er(Y) and two Fe atoms), (iii) used generalized angles $\Omega_{i,j,k}$ as short-hand for the Cartesian angles $(\theta_{i,j,k}, \phi_{i,j,k})$, e.g.,

$$\begin{aligned}&\cos(\Omega_{i,j,k+1} - \Omega_{i,j,k}) \\ &\quad = \sin\theta_{i,j,k+1}\sin\theta_{i,j,k}\cos(\phi_{i,j,k+1} - \phi_{i,j,k}) \\ &\qquad + \cos\theta_{i,j,k+1}\cos\theta_{i,j,k},\end{aligned} \tag{3}$$

(iv) set the magnetic Fe-Fe exchange and applied fields equal to $B_{\rm EX}$ and B_A, respectively, with the magnetic field applied along $\Omega_H[=(\theta_H, \varphi_H)]$, and (v) denoted the site anisotropy by $K_{i.j.k}(\Omega_{i,j,k})$, which is nonzero only at Er sites. The precise form of the Er anisotropy will be described below. However, for present purposes, we note that thin multilayers can be represented by the 1D model,

$$\begin{aligned}\varepsilon_k = &-\tfrac{1}{6}(2\mu_{\rm FE})B_{\rm EX}[\cos(\Omega_{k+1} - \Omega_k) \\ &+ \cos(\Omega_k - \Omega_{k-1})] - \tfrac{2}{3}(2\mu_{\rm FE})B_{\rm EX} \\ &+ K_{.k}(\Omega_k) - (2\mu_{\rm FE})B_A\cos(\Omega_k - \Omega_H) \\ &+ \mu_{\rm Er}B_A\cos(\Omega_k - \Omega_H),\end{aligned} \tag{4}$$

provided all the spins in a given *x*-*y* monolayer are parallel to each other. Estimates of $B_{\rm EX}$ and the monolayer thickness $d\ (=a/2)$ used for the $REFe_2$ Laves compounds are given in Ref. 22. Finally, to minimize calculations, cyclic boundary conditions have been used. For example, if the number of monolayers in a repeating unit structure is given by $N = (N_{YFe_2} + N_{ErFe_2})$, then $\Omega_1 \equiv \Omega_{N+1}$.

As noted earlier, the magnetic anisotropy of the $ErFe_2/YFe_2$ multilayer films is generated primarily by the Er^{3+} ions.[23] Here there are two competing interactions: (i) the normal cubic crystal field interaction, arising from the interaction between the charge distribution of the RE 4*f* shell and the electric gradients within the Laves phase crystal and (ii) the growth-induced magneto-elastic interaction.[12] Both are electrostatic in origin. The origin and calculation of the Er^{3+} ion anisotropy in the Laves phase $REFe_2$ compounds has been discussed in Refs. 23 and 24. Following the latter, the Er^{3+} crystal field anisotropy can be written in the concise form

$$\begin{aligned}K(\theta,\phi) = &\tilde{K}_4(T)\boldsymbol{Y}_4^C + \tilde{K}_6(T)\boldsymbol{Y}_6^C + \tilde{K}_8(T)\boldsymbol{Y}_8^C \\ &+ \tilde{K}_{10}(T)\boldsymbol{Y}_{10}^C + \tilde{K}_{12}(T)\boldsymbol{Y}_{12}^C.\end{aligned} \tag{5}$$

Here the $\boldsymbol{Y}_N^C$ are combinations of spherical harmonics with cubic symmetry (see table 3 of Ref. 24). Values of the temperature-dependent anisotropy parameters $\tilde{K}_n(T)$ for the Er^{3+} ion can be found in Fig. 4 of the same paper. In addition, several contributions to the temperature-dependent strain term are alluded to above (see Ref. 25). But for simplicity, we have only taken into account the first-order strain term $K_2'(T)$:

$$K_S(\theta,\phi) = K_2'(T)\frac{1}{2}\sqrt{\frac{15}{2\pi}}\sin^2\theta\sin 2\phi. \tag{6}$$

Values of the temperature-dependent $K_2'(T)$ for Er^{3+} can be found in Fig. 4 of Ref. 25. Finally, it should be noted that the anisotropy parameters are given with respect to the natural cubic axes of the $REFe_2$ unit cell. In practice, it is necessary to transform to a new coordinate system, in which the (x, y, z) axes coincide with ([00$\bar{1}$], [01$\bar{1}$], [110]) cubic axes [see Fig. 1]. Details of such transformations can be found in Ref. 26.

Of course, both the Fe and Er magnetic moments and the Fe-Fe magnetic exchange fields are themselves temperature dependent. Here, it is assumed that both the Fe and magnetic Fe-Fe exchange field $B_{\rm EX}$ follow the magnetic hyperfine field, as determined many years ago by the ^{57}Fe Mössbauer effect. Additionally, the magnetic moment at the Er site is determined by the Er-Fe magnetic exchange field. Full details can be found in Ref. 24.

We are now in a position to discuss the results of our micromagnetic simulations. Note that in zero field, the $ErFe_2/YFe_2$ multilayer adopts a simple layered AF state with the magnetic moment pointing out of the plane of the film, somewhere between the [110] growth direction and, say, the out-of-plane [11$\bar{1}$] axis.

V. MICROMAGNETIC SIMULATIONS

First, we stress that the parameters discussed in the previous section were not adjusted to fit the XMCD data. Second, in a complex magnetic system such as an exchange-spring magnet, several stable spin arrangements can exist at a given field and temperature. An example can be seen in Fig. 5(a). It will be observed that there are two stable spin configurations: the

vertical exchange-spring state (blue, outer loop) and the spin-flop state (red, inner line). In practice, the latter cannot be reached starting from a high magnetic field value. In this case, therefore, our interest lies in a determination of the switching field, between the vertical exchange spring and its reversed state.

There are two possible methods by which switching fields can be determined. First, the range of stability for a particular state is determined. Going beyond the stability range, the magnetic system must perforce switch into another spin state. In Fig. 5(a), the outer dotted lines at ±5.12 T signal the limits of the stability range of the vertical exchange-spring state (i.e., $B_{i.\,\mathrm{max}} \pm 5.12$ T). This upper limit resembles that of the Stoner-Wohlfarth model, except that the magnetization is now nonuniform. Second, a lower limit of the switching field can be established by assuming the system switches when the energies of the vertical exchange state and its reverse state become identical (i.e., $B_{i.\,\mathrm{min}} \pm 2.04$ T [see inner dotted lines of Fig. 5(a)]). Clearly, the actual switching field must lie somewhere between these two values. As a working model, we have taken the value of the switching field to be the simple average of these two limiting cases (i.e., $B_c = {}^1\!/_2[(B_{i.\,\mathrm{max}} + B_{i,\,\mathrm{min}})] = 3.58$ T). For the remainder of the simulation data presented below, we shall show only the average values of the switching fields. In practice, it is found that this procedure provides values of the switching field in reasonable agreement with the experiment. The expected Er magnetization curve can be seen in Fig. 5(b). This shows a striking similarity with the Er-XMCD loop obtained at 150 K

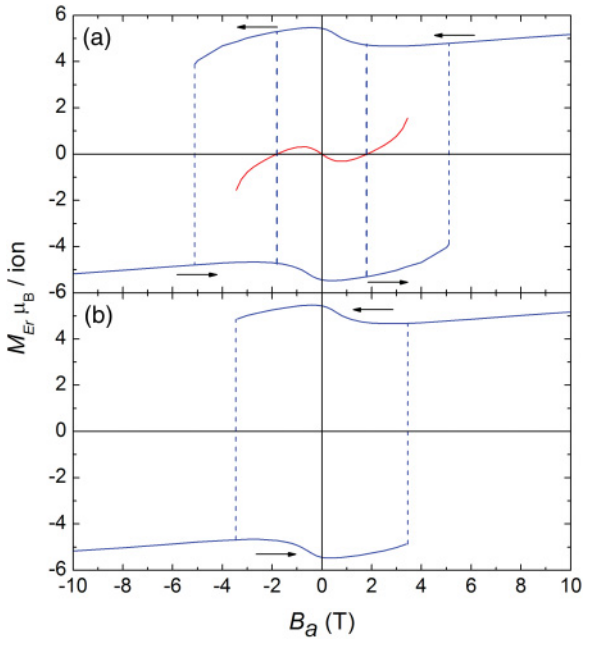

FIG. 5. (Color online) (a) Simulated M_{Er}-B_{a} magnetic hysteresis loop at 150 K. Solid blue lines correspond to vertical (spin-flop) exchange-spring states. The vertical outer dashed lines at 5.12 T (blue) correspond to $B_{i,\mathrm{max}}$. The inner dashed lines (blue) at 2.04 T are where the energy of the two spring states is identical, $B_{i,\mathrm{min}}$. The solid red line at $B_a = 0$, $M_{\mathrm{Er}} = 0$ gives the M_{Er} stable spin-flop states. (b) Expected M_{Er}-B_{a} loop at 150 K using the average switching field $B_{\mathrm{c}} = 3.58$ T.

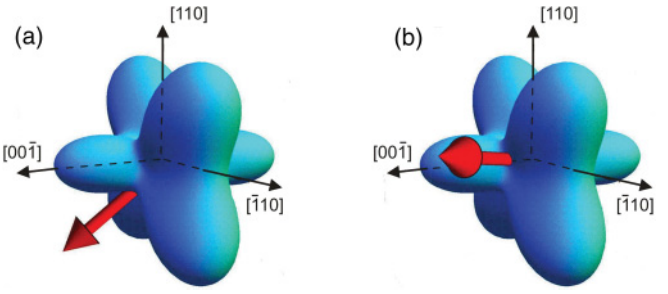

FIG. 6. (Color online) Average Er moment (red) obtained from the simulations with respect to the single-ion anisotropy energy surface (blue) for (a) the vertical exchange-spring and (b) the spin-flop state.

shown in Fig. 2(c). Note that both curves show an increase in M_z as the applied magnetic field passes through zero, as found experimentally.

It is also of some interest to examine the direction of the average Er^{3+} magnetic moment for the two states described above. Note that calculation shows that both states can exist at 150 K in a field of 4 T [see Fig. 5(a)]. The direction of the average Er moment is illustrated schematically in Fig. 6. Note the switch from being out of plane to in plane, on switching from the vertical exchange-spring state to its spin-flop counterpart.

However, in going from 150 to 200 K, the overall shape of the simulated M_{Er}-B_a loop changes dramatically. At the higher temperature, there are now two distinct magnetic switching fields. Once again, we have used the simple average switching fields to produce the magnetization curves shown in Figs. 7(a) and 7(b). As the temperature is increased, micromagnetic

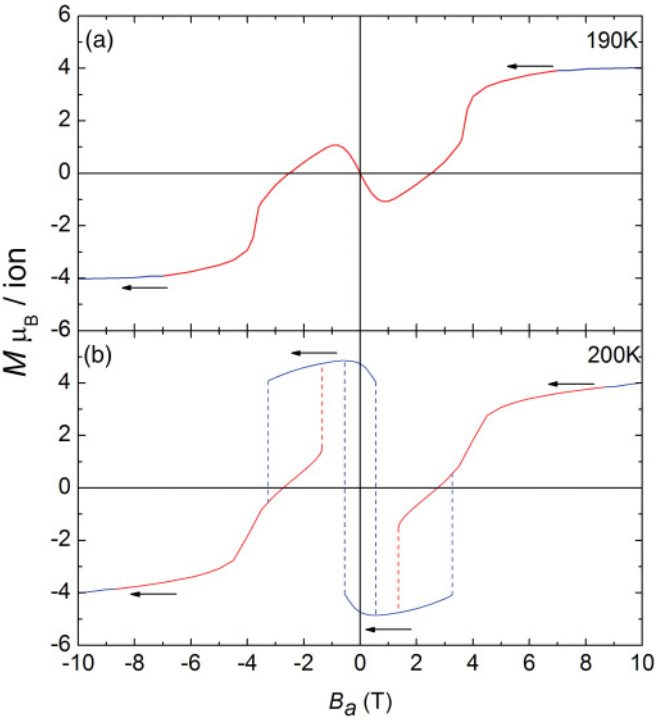

FIG. 7. (Color online) Simulated Er magnetization curves at (a) 190 K and (b) 200 K.

simulation predicts that there should be a crossover from a single-switch to double-switch magnetic loop, as shown in Fig. 7(b). In the XMCD experiments, this occurs at 220 K. However, the best agreement is found for simulation data at slightly lower temperatures. This difference may be due to inaccuracies in the values used for Er^{3+} anisotropy parameters.

It should also be noted that, although at low and high temperatures the agreement between experimental and simulation data is good, there is only qualitative agreement in the shapes of the magnetization curves in the crossover regime. Here the simulated data show relatively little in the way of hysteresis, whereas this is not the case in the measured Er-XMCD curve. This behavior may be due either to the anisotropy associated with the YFe_2 layers or dipole-dipole interactions neglected in micro-magnetic simulations using cyclic boundary conditions. These may cause some disagreement between theory and experiment, particularly at those temperatures where the energies of the different states are finely balanced.

Finally, calculations have also been performed using a 1D model with up to ∼20 bilayer repeats, but with no cyclic boundary conditions in the z direction. This allows Er magnetization curves to be computed from, say, the top $ErFe_2$ layer, as opposed to that of the bulk. The results reveal that although the computed switching field can change by ∼10–20%, the z magnetization of the top $ErFe_2$ layer differs from that of the bulk by only a few percent.

VI. INSTABILITIES

From the above, it is clear that certain spin configurations become unstable at certain temperatures and fields. In the computational studies, such singular points are established by examining the double-derivative matrix E''_{total} of the total energy $\boldsymbol{E}_{\text{total}}$, as detailed in Ref. 27. If all eigenvalues of E''_{total} are positive, the spin configuration defined by the set of angles $\{\theta_i,\varphi_i\}$ represents a stable spin configuration. On the other hand, if any of the eigenvalues is negative, the spin configuration is unstable, representing an energy maximum rather than minimum. Such techniques therefore offer a mathematical procedure not only to identify but to shed light on the nature of such instabilities.

The field dependence of the average inclination angle $\langle\theta\rangle_{\text{Er}}$ for the Er moments at 190 K and 220 K below and above the spin-flop transition can be seen in Fig. 8. All curves are for the spin-flop exchange-spring states. The data for 190 K reveal a continuous curve (lower solid curve) for the field range in question. Here the spin-flop state is stable for all the fields studied. However, when the temperature is raised to 220 K (upper dotted curve), a field-range appears (0.19 → 2.17 T) where the spin-flop state is unstable. In this field region, the magnetic spin configuration must perforce collapse into a vertical exchange-spring spin configuration.

To provide further insight into the nature of the instability, we have examined the spin-flop instability at 200 K. The results can be seen in Fig. 9. This time, we have plotted both the average angle $\langle\theta\rangle_{\text{Er}}$ and $\langle\phi\rangle_{\text{Er}}$ of the Er moments as a function of magnetic field. Starting from a high field of 10 T, only the vertical exchange-spring state is stable. Here $\langle\theta\rangle_{\text{Er}}$ is ∼40°, whereas $\langle\phi\rangle_{\text{Er}}$ is zero. But as the field is lowered below 8.7 T, $\langle\phi\rangle_{\text{Er}}$ suddenly becomes nonzero. We

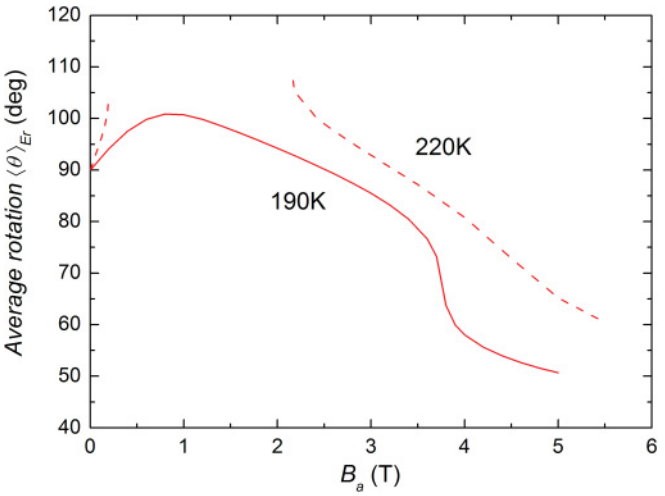

FIG. 8. (Color online) Average $\langle\theta\rangle_{\text{Er}}$ corresponding to stable spin-flop states at 190 K (solid line) and 220 K (dotted line).

identify this as signifying the onset of the spin-flop phase with a y component. This transition is second order in character, signifying a gentle rotation by the spin configuration away from the z-x plane. However, as the magnetic field is lowered further, $\langle\phi\rangle_{\text{Er}}$ grows in magnitude, reaching ∼45°, until finally undergoing a discontinuous (first-order) transition at 1.3 T. In essence, the parameter $\langle\phi\rangle_{\text{Er}}$ acts as an order parameter distinguishing the two states: $\langle\phi\rangle_{\text{Er}} = 0$ for the vertical spring state and $\langle\phi\rangle_{\text{Er}} \neq 0$ for the spin-flop state.

Further investigation of the relationship between the direction of the average Er moment and its associated anisotropy field reveals that at 200 K, for an applied field decreased from high fields to 3 T, the average Er moment is located in a small energy minimum, associated with an in-plane ⟨111⟩-type axis (see Fig. 6). But as the field is reduced to 1.3 T, the Er moment rotates steadily downward ($\langle\theta\rangle_{\text{Er}}$ increasing, $\langle\phi\rangle_{\text{Er}}$ decreasing), eventually overriding the small energy saddle point between the in-plane and out-of-plane ⟨111⟩-type axes. When this occurs, the spin configuration collapses into a vertical spring state, as observed in the XMCD data. At

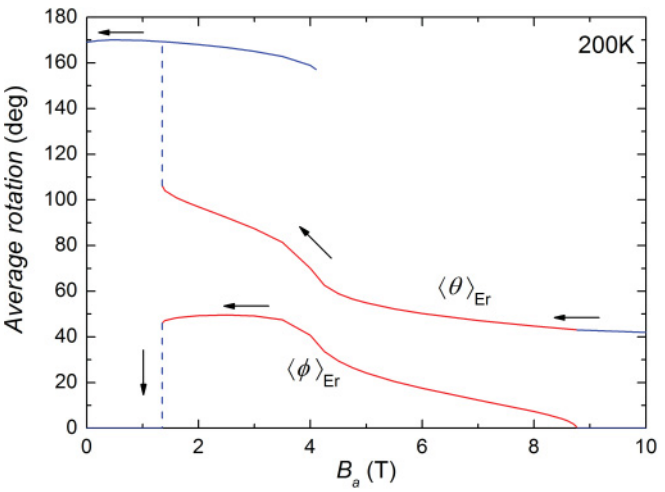

FIG. 9. (Color online) (a) Average $\langle\theta\rangle_{\text{Er}}$ and $\langle\varphi\rangle_{\text{Er}}$ corresponding to stable states at $T = 200$ K.

220 K, the energy barrier in question is small. We find that the anisotropy barrier is $\Delta E = 0.051$ K per Er ion. However at 190 K, the energy barrier has increased to $\Delta E = 0.182$ K per Er ion. This threefold increase is sufficient to trap Er moments in the energy-minimum-associated vertical exchange-spring state in the magnetic hysteresis loop. In short, the geometrical shape of the Er^{3+} single-ion anisotropy curve plays a major role in the pinning/depinning of the vertical and spin-flop exchange-spring states.

VII. CONCLUSIONS

XMCD measurements at the Er $M_{4,5}$ edge using electron drain current detection have been performed, yielding valuable information about the switching processes in $ErFe_2/YFe_2$ exchange-spring superlattices. It was found that magnetization switching transitions at high temperatures, insignificant in bulk magnetometry data due to the nearly complete cancellation of the magnetization of hard and soft layers,[10] are much more pronounced in the magnetization curves of the Er ions. The experiments confirm the crossover from a relatively simple single switching behaviour for $T < 200$ K to double-switching for $T > 220$ K, originally inferred from bulk magnetometry.

Micromagnetic modeling, using the discrete 1D model for finding minimum energy states, gives good agreeement with the XMCD data. The origin of double-switching has been traced to instabilities in *both* the spin-flop configuration and vertical spring configuration at temperatures of ∼200 K. These, in turn, can be associated with the geometrical shape of the Er^{3+} single-ion anisotropy. Depinning of exchange-spring states is determined primarily by low-energy saddle points, which allow the Er magnetic moments to change direction without riding up over the much larger anisotropy maxima.

In summary, hard-layer-specific magnetometry enabled by XMCD and combined with micromagnetic modeling offers valuable opportunities to investigate magnetization states and switching processes in complex multilayer systems. In particular, in $ErFe_2/YFe_2$ superlattices, the discrete 1D model has been used to show that the magnetic states associated with the switching event can be classified in two types. At low temperatures, in standard magnetic hysteresis loops, only vertical exchange-spring states are traversed. Here, all the magnetic moments are confined to the $(\bar{1}10)$ plane. However, at temperatures above a crossover temperature regime of around 200 K, other magnetization states play a role. Such states have magnetic components pointing out of the $(\bar{1}10)$ plane with a hard-layer magnetization close to the film plane. These states bear a strong similarity to spin-flop states in classical antiferromagnets, in which an increase in anisotropy energy is overcome by a decrease in Zeeman energy. By way of contrast, in the $ErFe_2/YFe_2$ superlattices, the increases in both the Er anisotropy and Fe-Fe exchange energy are overcome by an overall decrease in Zeeman energy of both the Er ions and YFe_2 exchange springs. As a result, multilayers can undergo exchange-spring-driven transitions between vertical and spin-flop states, and vice versa.

*gbgs1g09@soton.ac.uk

[1] D. Suess, T. Schrefl, R. Dittrich, M. Kirschner, F. Dorfbauer, G. Hrkac, and J. Fidler, J. Mag. Mag. Mater. **290**, 551 (2005).

[2] D. Suess, T. Schrefl, S. Fahler, M. Kirschner, G. Hrkac, F. Dorfbauer, and J. Fidler, Appl. Phys. Lett. **87**, 012504 (2005).

[3] R. H. Victora and X. Shen, IEEE Trans. Mag. **41**, 537 (2005).

[4] R. Skomski and J. M. D. Coey, IEEE Trans. Mag. **29**, 2860 (1993).

[5] R. Skomski and J. M. D. Coey, Phys. Rev. B **48**, 15812 (1993).

[6] M. R. J. Gibbs, J. Magn. Mag. Mater. **290**, 1298 (2005).

[7] A. Ludwig and E. Quandt, J. Appl. Phys. **87**, 4691 (2000).

[8] C. T. Pan and S. C. Shen, J. Mag. Mag. Mater. **285**, 422 (2005).

[9] K. Dumesnil, M. Dutheil, C. Dufour, and Ph. Mangin, Phys. Rev. B **62**, 1136 (2000).

[10] K. N. Martin, K. Wang, G. J. Bowden, A. A. Zhukov, P. A. J. de Groot, J. P. Zimmermann, H. Fangohr, and R. C. C. Ward, Appl. Phys. Lett. **89**, 132511 (2006).

[11] K. N. Martin, C. Morrison, G. J. Bowden, P. A. J. de Groot, and R. C. C. Ward, Phys. Rev. B **78**, 172401 (2008).

[12] A. Mougin, C. Dufour, K. Dumesnil, and Ph. Mangin, Phys. Rev. B **62**, 9517 (2000).

[13] K. Dumesnil, C. Dufour, Ph. Mangin, A. Rogalev, and F. Willhelm, J. Phys.: Condens. Matt. **17**, 215 (2005).

[14] K. Dumesnil, S. Fernandez, A. Avisou, C. Dufour, A. Rogalev, F. Willhelm, and E. Snoeck, Eur. Phys. J. B **72**, 159 (2009).

[15] J. P. Zimmermann, G. Bordignon, R. P. Boardman, T. Fishbacher, H. Fangohr, K. N. Martin, G. J. Bowden, A. A. Zhukov, and P. A. J. De-Groot, J. Appl. Phys. **99**, 08B904 (2006).

[16] M. J. Bentall, R. C. C. Ward, E. J. Grier, and M. R. Wells, J. Phys.: Condens. Matt. Phys. **15**, 6493 (2003).

[17] C. Wang, A. Kohn, S. G. Wang, and R. C. C. Ward, J. Phys.: Condens. Matter **23**, 116001 (2011).

[18] B. T. Thole, G. van der Laan, J. C. Fuggle, G. A. Sawatzky, R. C. Karnatak, and J. M. Esteva, Phys. Rev. B **32**, 5107 (1985).

[19] G. van der Laan and B. T. Thole, Phys. Rev. B **43**, 13401 (1991).

[20] G. J. Bowden, A. R. Buckingham, G. B. G. Stenning, and P. A. J. de Groot, J. Condens. Matt. Phys. **22**, 291001 (2010).

[21] M. S. S. Brooks, L. Nordstrom, and B. Johansson, J.Phys.: Condens. Matt. **3**, 2357 (1991).

[22] G. J. Bowden, K. N. Martin, B. D. Rainford, and P. A. J. De-Groot, J. Phys: Condens. Matt. **20**, 015209 (2008).

[23] U. Atzmony and M. P. Dariel, Phys. Rev. B **13**, 4006 (1976).

[24] K. N. Martin, P. A. J. de Groot, B. D. Rainford, K. Wang, G. J. Bowden, J. P. Zimmermann, and H. Fangohr, J. Phys.: Condens. Matt. **18**, 459 (2006).

[25] G. J. Bowden, P. A. J. de Groot, B. D. Rainford, K. Wang, K. N. Martin, J. P. Zimmermann, and H. Fangohr, J. Phys.: Condens. Matt. **18**, 5861 (2006).

[26] G. J. Bowden, K. N. Martin, A. Fox, B. D. Rainford, and P. A. J. De-Groot, J. Phys: Condens. Matt. **20**, 285226 (2008).

[27] G. J. Bowden, J.-M. L. Beaujour, A. A. Zhukov, B. D. Rainford, P. A. J. de Groot, R. C. C. Ward, and M. R. Wells, J. Appl. Phys. **93**, 6480 (2003).